# Seafloor seismicity, Antarctic ice-sounds, cetacean vocalizations and long-term ambient sound in the Indian Ocean basin

J.-Y. Royer,[1] R. Chateau,[1] R.P. Dziak[2] and D.R. Bohnenstiehl[3]

[1]*CNRS and University of Brest, Laboratoire Domaines Océaniques, Brest, France. E-mail: jean-yves.royer@univ-brest.fr*
[2]*NOAA/Pacific Marine Environment Laboratory, CIMRS/Oregon State University, Newport, OR, USA*
[3]*Department of Marine, Earth and Atmospheric Sciences, North Carolina State University, Raleigh, NC, USA*

## SUMMARY

This paper presents the results from the Deflo-hydroacoustic experiment in the Southern Indian Ocean using three autonomous underwater hydrophones, complemented by two permanent hydroacoustic stations. The array monitored for 14 months, from November 2006 to December 2007, a 3000 × 3000 km wide area, encompassing large segments of the three Indian spreading ridges that meet at the Indian Triple Junction. A catalogue of 11 105 acoustic events is derived from the recorded data, of which 55 per cent are located from three hydrophones, 38 per cent from 4, 6 per cent from five and less than 1 per cent by six hydrophones. From a comparison with land-based seismic catalogues, the smallest detected earthquakes are $m_b$ 2.6 in size, the range of recorded magnitudes is about twice that of land-based networks and the number of detected events is 5–16 times larger. Seismicity patterns vary between the three spreading ridges, with activity mainly focused on transform faults along the fast spreading Southeast Indian Ridge and more evenly distributed along spreading segments and transforms on the slow spreading Central and ultra-slow spreading Southwest Indian ridges; the Central Indian Ridge is the most active of the three with an average of 1.9 events/100 km/month. Along the Sunda Trench, acoustic events mostly radiate from the inner wall of the trench and show a 200-km-long seismic gap between 2 °S and the Equator. The array also detected more than 3600 cryogenic events, with different seasonal trends observed for events from the Antarctic margin, compared to those from drifting icebergs at lower (up to 50°S) latitudes. Vocalizations of five species and subspecies of large baleen whales were also observed and exhibit clear seasonal variability. On the three autonomous hydrophones, whale vocalizations dominate sound levels in the 20–30 and 100 Hz frequency bands, whereas earthquakes and ice tremor are a dominant source of ambient sound at frequencies <20 Hz.

**Key words:** Hydrogeophysics; Acoustic properties; Mid-ocean ridge processes; Indian Ocean.

## 1 INTRODUCTION

Due to the remoteness of most mid-ocean ridges relative to the continents, the low-level seismic activity associated with the seafloor spreading processes is often not well recorded by land-based seismic networks. This is due to the rapid attenuation of seismic waves in the solid Earth, which prevents small magnitude earthquakes from being detected at distant land-based stations. Acoustic waves in the oceans, however, can propagate sound over very long distances with little attenuation. Exploiting this exceptional acoustic environment, deployments of hydrophone arrays have been used effectively to monitor the acoustic waves generated by submarine seismic and volcanic activity (Dziak *et al.* 2012). The low-level background seismicity of mid-ocean ridges has been so monitored

for 20 yr in the Pacific Ocean (e.g. Fox *et al.* 1995; Fox & Dziak 1998; Fox *et al.* 2001; Dziak *et al.* 2011) as well as in the Atlantic Ocean (e.g. Smith *et al.* 2002; Bohnenstiehl *et al.* 2003; Dziak *et al.* 2004; Goslin *et al.* 2005; Simão *et al.* 2010; Goslin *et al.* 2012). The Indian Ocean offers the opportunity to simultaneously monitor the low-level seismic and volcanic activity of three ridges with contrasting spreading rates, from ultraslow to slow and intermediate, respectively, along the Southwest, Central and Southeast Indian Ridges that meet at the Indian triple junction (Schlich 1982). From October 2006 to January 2008 (14 months), an array of three autonomous underwater hydrophones (AUHs) was deployed as part of the Deflo (Deformation of the Oceanic Lithosphere) experiment. These data have been analyzed in conjunction with data from two permanent hydroacoustic stations of the International Monitoring
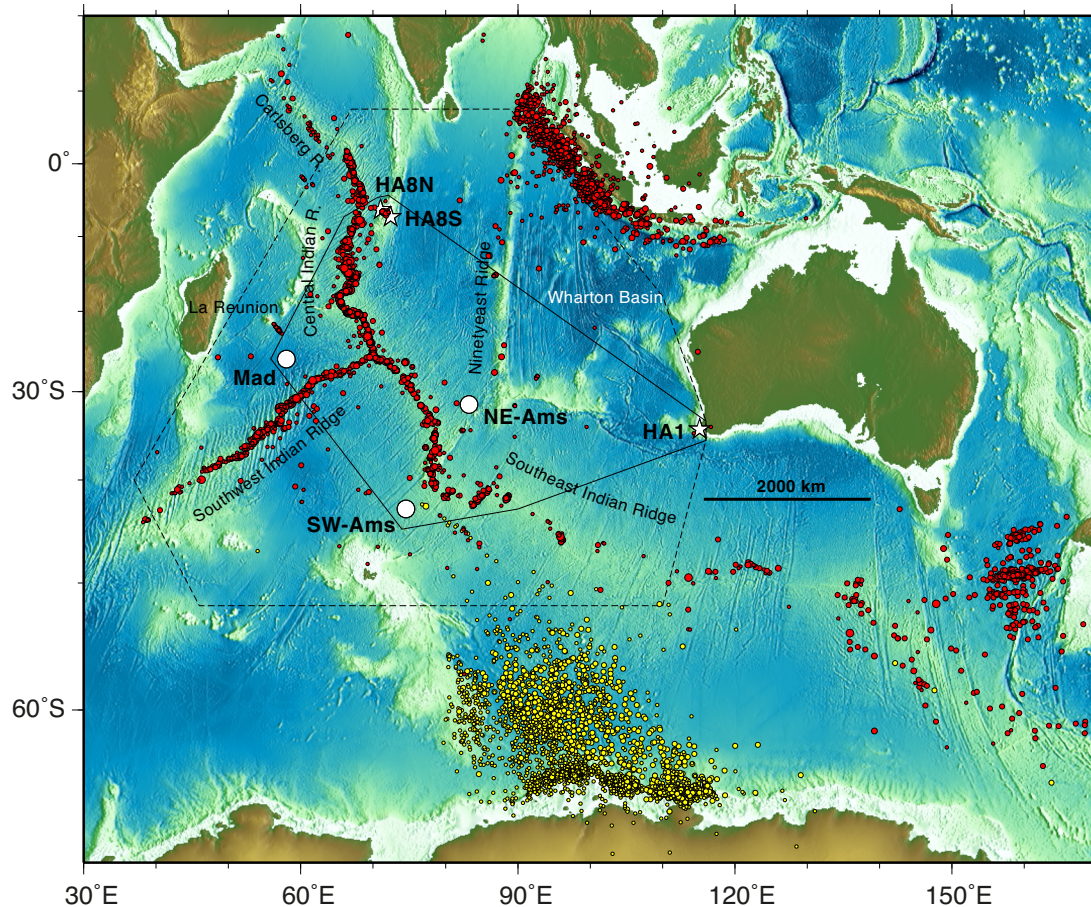
**Figure 1.** Acoustic events detected between 2006 October 1 and 2008 January 31 by an array of three temporary hydrophones (open circles) and three permanent IMS hydroacoustic stations (open stars). Yellow symbols refer to icequakes or cryogenic tremors. Size of symbol reflects the number of hydrophones (from 3 to 6) used in the location determination. Polygons refer to event analyses in the text.

System (IMS) of the Comprehensive Nuclear-Test-Ban Treaty Organization (CTBTO), which have been used previously to assess the soundscape in the Indian Ocean basin (Hanson & Bowman 2005, 2006). This paper presents the data acquired during the Deflo experiment and the cataloguing of seismic and volcanic events, whale vocalizations, icequakes and cryogenic tremors.

## 2 DATA ACQUISITION

The array of hydrophones was set to encompass the three Indian ocean spreading ridges with instruments located south of La Reunion Island in the Madagascar Basin (MAD), mid-way between the Kerguelen and Amsterdam islands (SW-AMS), and northeast of the St Paul and Amsterdam volcanic plateau (NE-AMS; Fig. 1). These three AUHs were deployed in October 2006 during a survey of the St Paul and Amsterdam plateau. Two of the instruments were recovered during a cruise in January 2008 and the third was recovered in April 2008 during yearly supply voyage to the French southern islands. In total, this remote hydroacoustic experiment required 110 d at sea to complete. The instruments were moored in the SOFAR (Sound Fixing and Ranging) channel axis at depths ranging from 1300 to 1000 m (Table 1). The Pacific Marine Environment Laboratory (NOAA/PMEL) provided the AUHs, and Laboratoire Domaines Océaniques supplied the moorings.

The hydrophones were set to record acoustic waves continuously at a rate of 250 Hz on 2-byte-long samples (16 bits A/D converter).

Their Q-Tech high-precision clocks were synchronized with the GPS clock prior to deployment and after recovery. Clock drift range from 0.8 to 1.5 s over about 14 months (i.e. average drift in the order of $10^{-8}$; Table 1). The permanent IMS hydroacoustic stations, located on either side of Diego Garcia Island (HA08N, HA08S) and off Cape Leeuwin (HA01W) Australia, complemented our temporary array. Although each of them actually comprises a triplet of hydrophones, 2 km apart from one another and cabled to shore, our analysis used only one hydrophone of each triad. The IMS acoustic records are similarly sampled at 250 Hz. With this set of three temporary and three permanent stations (at five sites), the whole array encompassed an area of approximately 3000 × 3000 km, but detected events cover a much wider area from the Antarctic margin (70°S) to the northern termination of the Sunda Trench (10°N), and from 35°E to the Macquarie Ridge (160°E; Fig. 1).

## 3 CATALOGUE OF HYDROACOUSTIC EVENTS

Data from the three AUHs and three IMS hydrophones were jointly analysed using the 'Seas' software developed at PMEL (Fox *et al.* 2001). The main task is to identify records of the same acoustic event on each instrument. The source of acoustic events is then localized by a non-linear least-square minimization of the arrival times (of peaks of energy in the spectrograms) on each of the hydrophones (Fox *et al.* 2001). Sound velocities in the ocean

**Table 1.** Autonomous hydrophone locations and parameters (jd = Julian day).

| Site | MAD | SW-AMS | NE-AMS |
|---|---|---|---|
| Hydrophone # | H22 | H11 | H40 |
| Latitude | 26°05.00′S | 42°59.46′S | 31°35.09′S |
| Longitude | 058°08.56′E | 074°35.34′E | 083°14.89′E |
| Depth | 1300 m | 1050 m | 1200 m |
| Record start | 2006 October 30 (08h59′) jd = 303 | 2006 October 11 (16h36′) jd = 284 | 2006 October 10 (15h39′) jd = 276 |
| Record end | 2008 January 5 (04h10′) jd = 005 | 2008 January 13 (05h13′) jd = 012 | 2008 April 26 (02h24′) jd = 117 |
| Clock drift | 1.52 s ($4 \times 10^{-8}$ s/s) | 1.28 s ($3 \times 10^{-8}$ s/s) | 0.80 s ($2 \times 10^{-8}$ s/s) |
| Data file size | 17.35 Gb | 18.45 Gb | 22.90 Gb |
| Sampling rate | 250 Hz | 250 Hz | 250 Hz |
| Sensitivity | −153.735 dB | −153.735 dB | −153.735 dB |

are derived from the Global Digital Environment Model (GDEM) and averaged along great circles joining the source and each of the receivers. A total of 11105 acoustic events were handpicked and localized from this hydrophone array (Fig. 1). In this collection, 5579 events (55 per cent) were localized with only three hydrophones, 3856 events (38 per cent) with four hydrophones, 591 events (6 per cent) with 5 hydrophones and only 79 events with six hydrophones; depending on the event locations, areas of shallow bathymetry may block acoustic propagation along some source-receiver paths. With more than three arrival times, uncertainties can be estimated (Fig. 2): inside the array, 80 per cent of the events have uncertainties ($1\sigma$) less than 3 km both in latitude and longitude, and less than 2 s in the time origin. Among the events determined from five and six hydrophones, 73 per cent (62 per cent with four hydrophones) have uncertainties in origin time that are less than 1s.

In an attempt to assess the accuracy of our event determination, we compared the Deflo catalogue with several catalogues from land-based seismological networks: the National Earthquake Information Center (NEIC) at the USGS, the global Centroid Moment Tensor catalogue (CMT), the earthquakes relocated by the International Seismological Center (ISC; 2011), the events relocated with the Engdahl *et al.* (1998) algorithm (EHB), and the Review Event Bulletin (REB) from the International Data Center of CTBTO. We limited this comparison to the area enclosed in our array (plain line polygon in Fig. 1), where location and time determinations are the most accurate. Thus this area comprises only shallow earthquakes (i.e. within the oceanic crust) for which the assumption is that the seismic/acoustic conversion point matches the epicentre location. For the period from 2006 October 3 to 2007 December 23, this area comprises 1905 acoustic events, 37 CMT events, 84 EHB events, 127 NEIC events, 128 ISC events and 265 REB events (Table 2). A search was made within a 100 s and 300 km window about each AUH event. The mean distance between the AUH and land-based seismic locations ranges from 11 to 18 km, with standard deviations of 8–16 km (Table 2). The median origin time delay (preferred to the mean to avoid outliers) ranges from 0.2 to –0.9 s except for the REB where it reaches –2.5 s; standard deviations are on the order of 6 s. A positive time-delay means a later T-wave origin-time relative to the hypocentre-time. The best matches are found with the EHB and CMT catalogues, which generally include the best-recorded events on land. This confirms an improved accuracy for the locations determined from the hydroacoustic data, relative to the teleseismic observations, as noted previously for AUH arrays in the Pacific and Atlantic Oceans (Bohnenstiehl & Tolstoy 2003; Pan & Dziewonski 2005).

Acoustic events can be characterized by their acoustic magnitude or source level. Source levels are derived from the recorded levels at each hydrophone, corrected from the transmission loss between the event and hydrophone locations. The received level (RL), expressed in decibels with respect to 1 micro-Pascal, (dB re μPa at 1 m) corresponds to the maximum peak-to-peak amplitude in a 10s-time window centred on the peak of energy in the acoustic signal, in the 3–110 Hz frequency range, which resembles most to the definition of seismic amplitudes. The transmission loss (TL) comes from the cylindrical sound-spreading between the event location and the hydrophone, and from the spherical sound-spreading in the water column between the sea-bottom acoustic radiator and the sound channel axis. Source level (SL) also with units of as dB re μPa at 1 m, is thus obtained from the following equation:

$$SL = RL + TL = RL + 10 \log(d) + 20 \log(z), \qquad (1)$$

where RL is the received level at the hydrophone, $d$ is the distance in kilometres between the event location and the hydrophone and $z$ is assumed constant and equal to 1000 m (i.e. a spherical spreading loss of 60 dB). The SL associated to an acoustic event will be the median value of the independently estimated SL's from each hydrophone; a median is preferred to a mean to avoid outliers due, for instance, to a low RL caused by a partially blocked acoustic path. In our catalogue, SL's range from 191 to 262 dB; in the dashed polygon in Fig. 1, the SL range from 212 to 252 dB and are centred on 221 dB.

The completeness of the hydroacoustic array can be assessed from the comparison of SL's with magnitudes of seismic events. This approach is based on the assumption that acoustic events follow a Gutenberg–Richter's law (1954) where SL's are, as magnitudes, proportional to the logarithm of the cumulative number of events with the same SL (e.g. Bohnenstiehl *et al.* 2002). Fig. 3 shows the distribution of SL and body-wave magnitude $m_b$ from land-based catalogues for all events in the polygon outlined in Fig. 1. Since the number of events and their $m_b$ magnitudes differ from one catalogue to another, the SL completeness, expressed in $m_b$, varies from 2.9 (EHB), 3.3 (REB), 3.2 (ISC) to 4.0 (NEIC). For comparison, the 'land-based' $m_b$ completeness for this area and period considered is 3.8 (REB), 4.0 (ISC, EHB) and 4.5 (NEIC). The SL completeness derived from the EHB catalogue is probably too low since the Engdahl *et al.* (1998) selection criteria exclude many smaller events within the ISC and other catalogues. The EHB catalogue does not estimate magnitude, and generally reports the same $m_b$ values as the ISC. For the selected events, the ISC and REB $m_b$'s are lower than the NEIC $m_b$'s, and the REB $m_b$'s are lower than the ISC $m_b$'s. Due to the distribution of IMS stations with respect to the other seismological arrays, the REB has magnitude of completeness that is 0.5 units smaller than the ISC catalogue (Storchak *et al.* 2011). Thus, for the area and period considered, the completeness of our hydrophone array is almost one magnitude unit (0.5–0.7) smaller than that of land-based seismological networks,
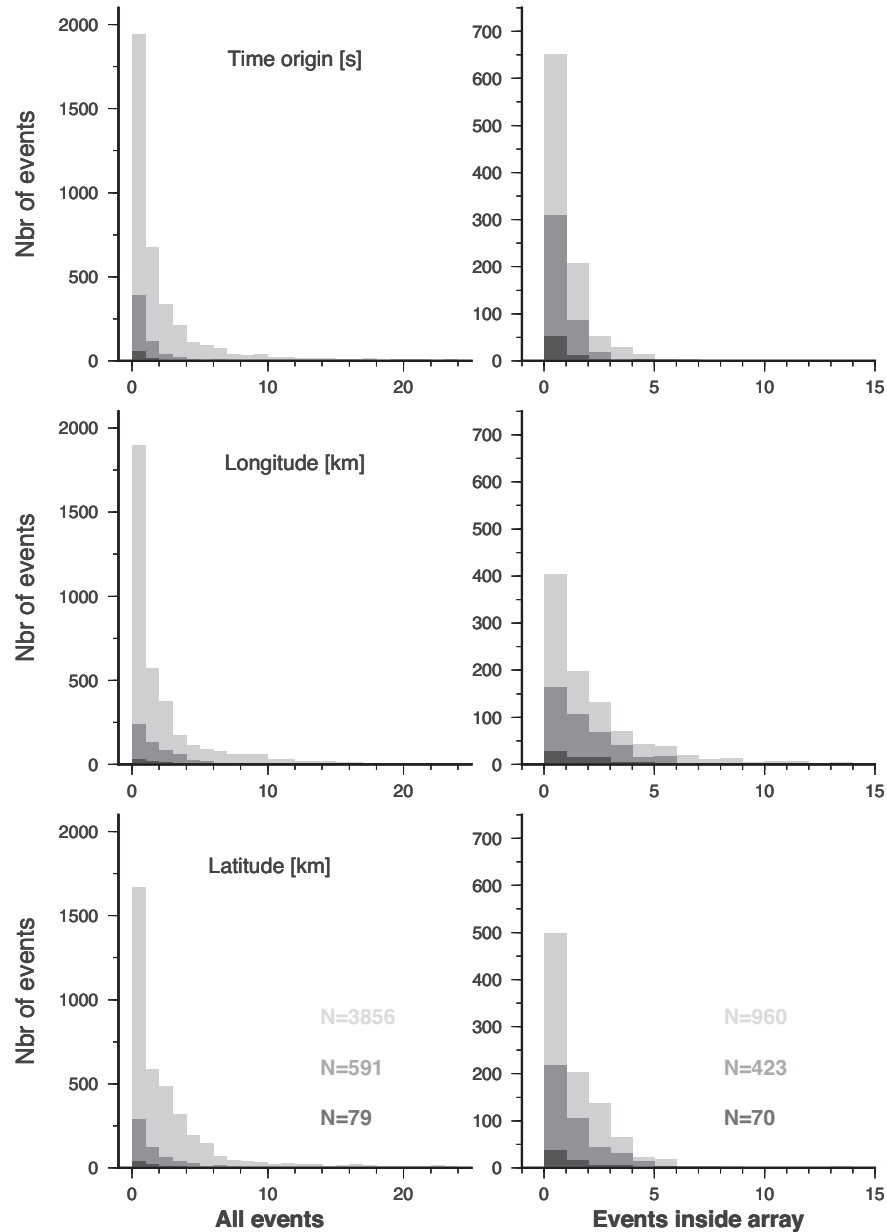
**Figure 2.** Distribution of uncertainties ($1\sigma$) in the location and time origin for all events (left-hand panel) and events located inside the hydrophone array (right-hand panel; events enclosed in dashed contour in Fig. 1); $N$ is the number of events detected by four hydrophones (light grey), five hydrophones (dark grey) and six hydrophones (black). Uncertainties cannot be calculated for events detected by only three hydrophones.

**Table 2.** Comparison between the AUH catalogue of events and land-based seismological catalogues (see text for the acronyms). Comparison limited to the 1905 acoustic events located inside the array (plain line polygon in Fig. 1), for the period between 2006 October 3 and 2007 December 23.

| Catalogue | REB | ISC | NEIC | EHB | CMT |
|---|---|---|---|---|---|
| Number of events | 265 | 128 | 127 | 84 | 37 |
| Matching events | 232 | 117 | 116 | 79 | 36 |
| Magnitude range | 3.4–5.1 | 3.6–5.6 | 3.8–5.9 | 3.8–5.6 | 4.6–5.8 |
| Mean distance | 18 km | 13 km | 13 km | 14 km | 11 km |
| Sigma | 16 km | 11 km | 10 km | 9 km | 8 km |
| Median time delay | –2.5 s | –0.4 s | –0.7 s | 0.2 s | –0.9 s |
| Sigma | 5.9 s | 5.8 s | 5.9 s | 4.7 s | 5.7 s |

leading to the detection of 5–16 times more events than the REB and NEIC networks, resp. ($\sim$10 times more than the ISC catalogue). From the comparison with the ISC catalogue, the lowest detected magnitude is in the order of $m_b$ 1.7 and the range of recorded magnitudes ($m_b = 1.7$–5.8) is about twice that of land-based networks ($m_b = 3.6$–5.8).

The catalogue consists of acoustic events mainly generated by earthquakes or volcanic eruptions along the Indian Ocean active plate boundaries, which are comprised of the three Indian spreading ridge system and the Sunda Trench; it also includes many ice quakes and iceberg-generated tremors located off the Antarctic margin. These events will be described in the next sections. Among
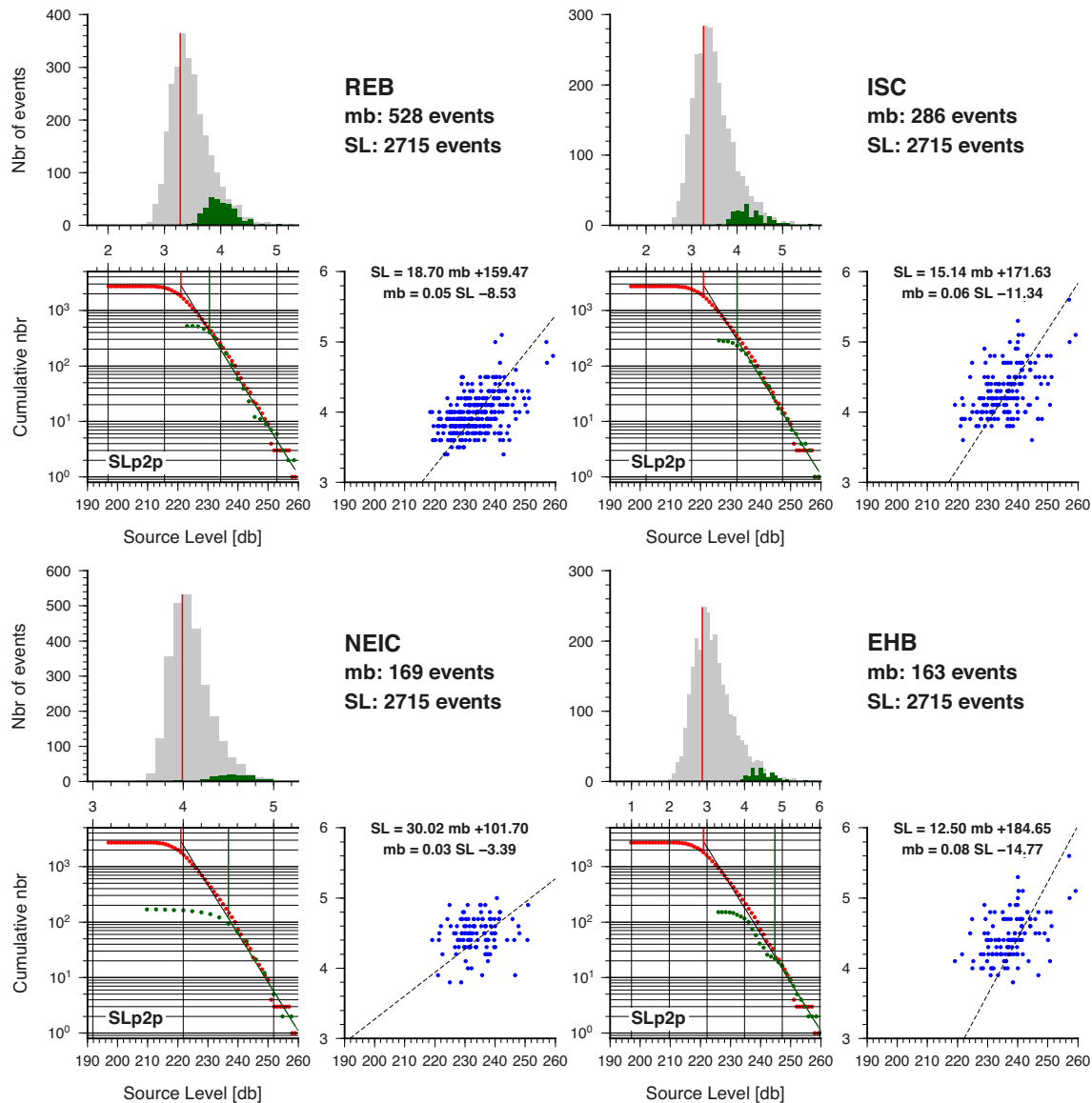
**Figure 3.** Comparison of acoustic Source Levels (SL) and seismic magnitudes ($m_b$) from different land-based catalogues, for events located inside the dashed-line polygon in Fig. 1. SLp2p is the SL peak to peak (see text). The correspondence between the SL and $m_b$ scales is based on matching the best-fitting Gutenberg–Richter lines up to the completeness values outlined in green for the land-based catalogues and in red for the acoustic catalogue. The upper graph shows the number of events in each catalogue in bins of $m_b = 0.1$ (it also shows the number of events relative to the SL scale). The maximum number of event (red line) corresponds to the acoustic completeness. The right graphs show the resulting SL to $m_b$ relationship (and reciprocal) and trend line. Note that the EHB catalogue adopts the ISC's $m_b$ values, whereas the ISC, NEIC and REB catalogues report different $m_b$ values for the same seismic events.

unusual events, on 2007 April 5, our array detected seismic activity associated with the eruption and collapse of the Piton de la Fournaise caldera on La Reunion Island (April 5; Michon *et al.* 2007). A total of 32 events (aligned dots near the island in Fig. 1) were recorded by the three autonomous hydrophones, two of them being about 3000 km away from the island. They span from April 5, 04h43 UTM to April 7, 15h10. Their SL is in the order of 220 dB except one event at 230 dB (April 6 at 17h23). Their mislocation and alignment with the southwestern edge of the array is a geometrical artefact of the localization inversion, whereby location accuracy decreases outside the array and locations tend to scatter along an azimuth, defined by a common travel-time hyperbole of events with similar arrival times across the array, that points toward the true source location

(Fox *et al.* 2001). There are also a few acoustic events in the middle of oceanic basins, for instance in the Crozet Basin (60–70°E, 40°S); their origin is unknown or they may be due to erroneous associations of events in the hydrophone records. However, all of the events located between the Central and Southeast Indian ridges and the Sunda Trench reflect the on-going intraplate deformation of the Indo-Australian Plate. They cluster near the Chagos Bank and Central Indian Ridge FZ's, off and east of the Southeast Indian Ridge, at the southern tip of the Ninetyeast Ridge, and over the Wharton Basin; all these areas are known to be seismically active (e.g. Bergman *et al.* 1984; Wiens 1986; Petroy & Wiens 1989) and form the diffuse plate boundaries between the rigid components of the Indo-Australian Plate (Royer & Gordon 1997).

## 4 MID-OCEANIC RIDGE SEISMICITY

The main objective of this experiment was to document the low-level seismic activity associated with the three Indian mid-oceanic ridges, which spread at contrasted rates from ultraslow (16 mm a$^{-1}$), slow (40 mm a$^{-1}$) to intermediate (65 mm a$^{-1}$), along the Southwest, Central and Southeast Indian ridges, respectively. The distribution of acoustic events along the three ridges is indeed contrasted. Figs 4–6 display the distribution of acoustic events versus their distance from the Rodrigues triple junction (RTJ) calculated from the best-fitting pole describing the relative motions along these plate boundaries (DeMets *et al.* 1994; NUVEL-1A); their geographic distribution are plotted in an oblique Mercator projection relative to these best-fitting poles. In such representation, events along transform faults will align along straight lines (i.e. will be at an equal distance from the RTJ).

Along the Southeast Indian Ridge (SEIR, 55–68 mm a$^{-1}$), the seismicity is mainly located on transform faults (TF) and occurs at an almost constant rate throughout the experiment duration (Fig. 4). The TF predominant activity is illustrated by stepwise increases in the cumulative number of events at FZ's (blue curve in Fig. 4). The most active area is the St Paul–Amsterdam (SPA) plateau (Fig. 7), which comprises several short ridge segments offset by closely spaced transforms (Royer & Schlich 1988; Conder *et al.* 2000; Scheirer *et al.* 2000; Maia *et al.* 2011). The active transforms are the Amsterdam FZ (78.6°E), bounding the SPA Plateau to the west, and two short transform offsets at 37.5°S and 38.7°S. On the 37.5°S TF, events align along both sides of a short, curved and presumably active ridge segment (Scheirer *et al.* 2000), suggesting the transform fault is continuous and that the curved ridge-segment is currently inactive. The SPA plateau also displays a large cluster of events (68 events in October 2007) at the western extremity of a long ridge segment and a small cluster (14 events in March 2007), clearly off axis and off transform, but centred on the St Pierre Bank, southeast of St Paul Island. No magmatic activity has yet been reported for this seamount. The only other active spreading segment on the SEIR is located 600 km from the RTJ (74.5°E).

Along the two other spreading ridges, seismicity of transform faults is still dominant but many ridge segments are also active, as illustrated by a regular increase in the cumulative number of events from the RTJ. The Central Indian Ridge (CIR, 48–35 mm a$^{-1}$) displays several very active ridge segments in the immediate vicinity of the triple junction and 150 km away from it, where active hydrothermal sites have been reported (Hashimoto *et al.* 2001; Van Dover *et al.* 2001). The next active segments are located between the Egeria and Marie Celeste FZ's (20–18°S) where active hydrothermal vents have recently been discovered (Tamaki 2010), and between 13° and 14°S, which comprises two short offset discontinuities. All transform faults are also very active. The seismicity of the Southwest Indian Ridge (SWIR, 14 mm a$^{-1}$) is even more evenly distributed in time and space, between transform and ridge segments, than the CIR. Swarms occur on two ridge segments at 58°E (January 2007, 1200 km) and 51°E (July/August 2007, 1800 km), and at the Atlantis II ridge-transform intersection at 57°E (January 2007, 1280 km; Figs 6 and 8). Small clusters of events also occur on off-axis parallel seamounts and could be associated with detachment faults parallel to the ridge axis (Sauter *et al.* 2013), as observed along the slow mid-Atlantic Ridge (Escartin *et al.* 2008); four events cluster on the Atlantis Bank, suggesting that the uplift of this transform-parallel seamount (Baines *et al.* 2003) is still on-going (Fig. 8).

Overall, within the range of SL (i.e. magnitudes) detected by the hydrophone array, the CIR is the most seismically active of three spreading ridges with an average of 28 events/100 km and 1.9 events/100 km/month, versus 20 and 1.3 for the SEIR and 18 and 1.2 for the SWIR (Table 3). Most events have SL values around $220 \pm 5$ dB, and, of the three ridges, the CIR has the largest number of events in this range. Within a 50 km radius, the Rodrigues triple junction concentrates a large number of events along the CIR (77), SWIR (20) and SEIR (11). The reduced number of events along the SEIR ridge segments may reflect a lesser seafloor spreading activity than along the CIR or SWIR, but is more likely due to the occurrence of events with SL's lower than the detection threshold of our hydrophones. The size of the largest spreading centre earthquakes is limited by the thickness of the brittle layer, and therefore decreases with increasing spreading rate (Cowie *et al.* 1993). The predominance of micro-earthquake ($M_L < 2$) activity along intermediate (e.g. Galapagos: Macdonald and Mudie 1974; Juan de Fuca: Hildebrand *et al.* 1997) and fast (e.g. East Pacific Rise: Stroup *et al.* 2007) spreading ridges is well established. The range of source levels is wider on transform faults (210–250 dB, up to 260 dB on the Marie-Celeste FZ, Fig. 5) than on ridge segments (210–240 dB).

## 5 SUBDUCTION SEISMICITY

A large number of acoustic events (3118) are located along the Sunda Trench (Fig. 9), of which one third (1064) are detected by 4 or more hydrophones (yellow symbols). The first observation is that most of the T-phase radiators related to subduction earthquakes are located along the continental wall of the trench, as shown by the best-located events (four hydrophones or more). The second observation is that they cluster in two main areas: near the hypocentres of the 2004 Aceh ($M_w = 9.0$) and 2005 Nias ($M_w = 8.7$) mega-events, and along a segment of the trench that ruptured in a series of large ($M_w > 6.9$) earthquakes in September 2007. Separating these two areas, there is a 200-km-long seismic gap. Between approximately 3° and 10°N, along the northern sections of the Aceh rupture zone (Lay *et al.* 2005; Tolstoy & Bohnenstiehl 2006), acoustic events occur in fewer numbers and they are located both along the trench and off the trench within the northern Wharton Basin. To the east and south of the 2007 events, earthquake activity becomes sparse in both the hydroacoustic and land-based (e.g. Engdahl *et al.* relocated events shown in Fig. 9) catalogues.

## 6 CRYOGENIC EVENTS

One surprise of this experiment was the numerous events (3645) of cryogenic origin recorded by our array, although many have been reported from the IMS stations, particularly from the HA01 station, off Cape Leeuwin, Australia (Hanson & Bowman 2005, 2006; Chapp *et al.* 2005; Gavrilov & Li 2008) or from seismological stations in the Pacific Ocean (Talandier *et al.* 2002, 2006). These events are mostly located southeast of Kerguelen Plateau and off the Antarctic margin (Figs 1 and 10). Some are clearly distinguishable from seismic events due to their duration (from a few 10 s to 30 min), larger frequency range (few Hz up to 100 Hz) or harmonic spectral character that may involve multiple overtones and exhibit time-frequency gliding (Fig. 10). The SOFAR channel becomes shallower at high latitudes and disappears to the south of the Antarctic Convergence Zone. Signals originating near the Antarctic coast must therefore
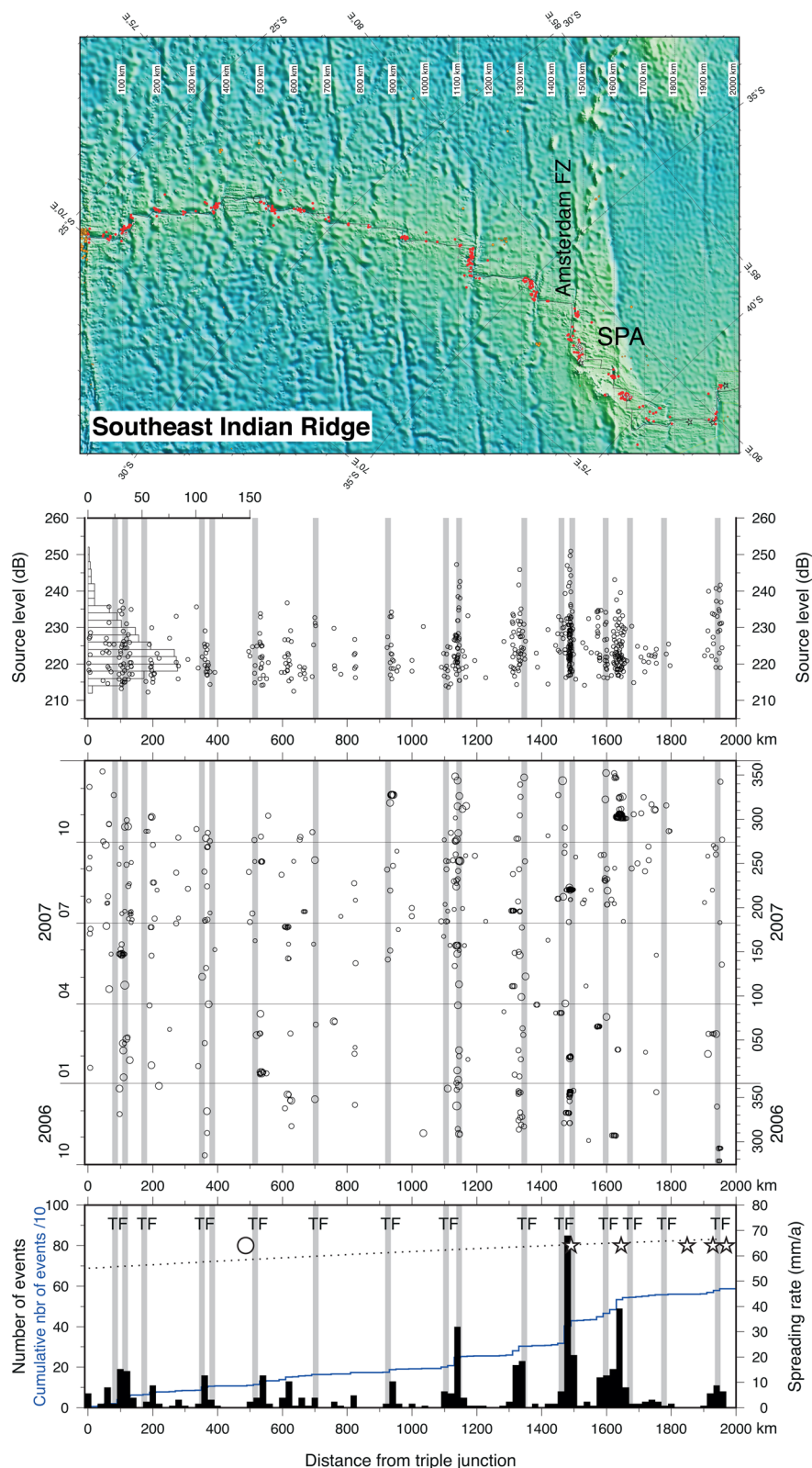
**Figure 4.** Distribution of acoustic events along the Southeast Indian Ridge (SEIR). Top panel: mid-oceanic ridge events in an oblique Mercator projection relative to the NUVEL-1A best-fitting pole for the SEIR (SPA: St Paul and Amsterdam Plateau). Straight lines correspond to small circles about the best-fitting pole; distances are reported from the Rodrigues triple junction (RTJ). Bottom panel: number, time and source level distributions of events versus distance from the RTJ calculated from NUVEL-1A best-fitting pole. Vertical grey lines are transform faults (TF). The dotted black line shows the spreading rates predicted by the kinematic model. The blue line corresponds to the cumulative number (divided by 10) of acoustic events from the RTJ. Large stars and circles correspond to hydrothermal sites reported as active (full star), inactive (open star) or inferred from plume anomalies in the water column (open circle) in the InterRidge data base (Beaulieu 2013).
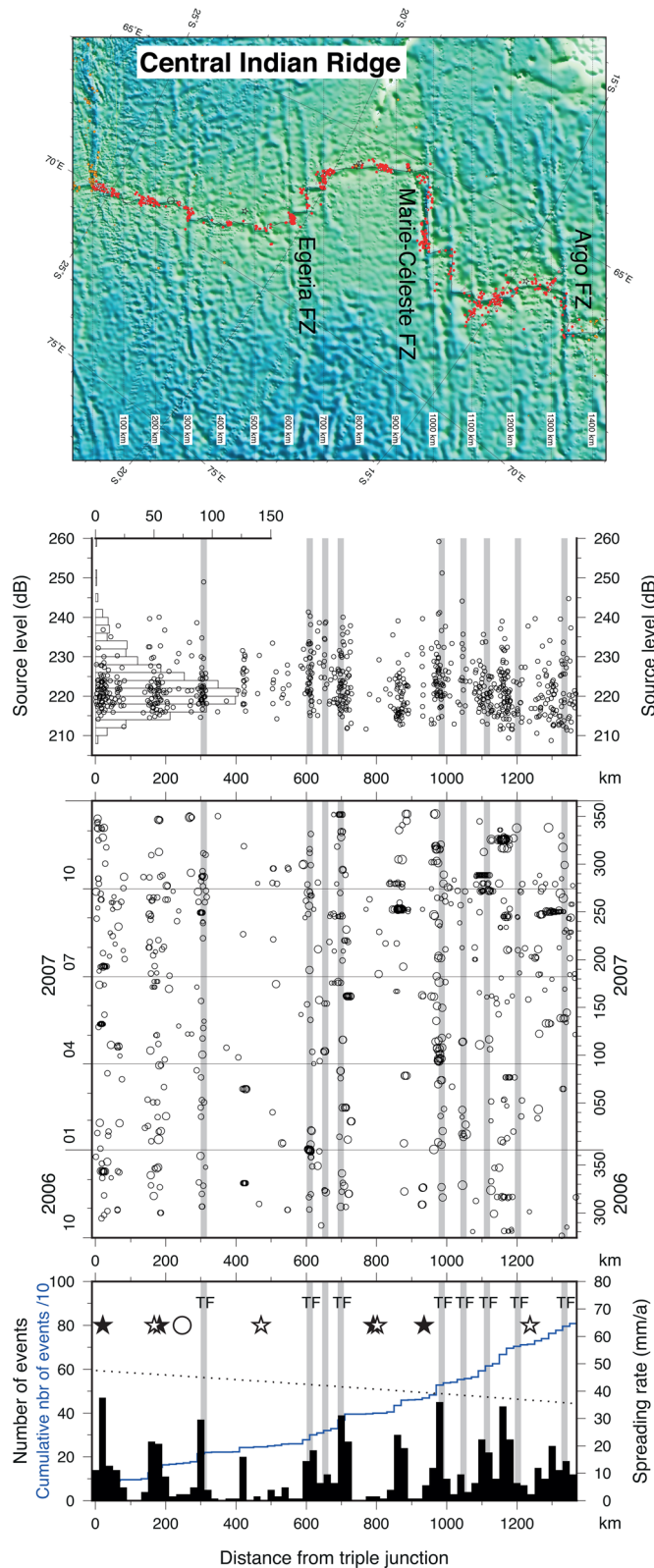
**Figure 5.** Distribution of acoustic events along the Central Indian Ridge (CIR). Same legend as in Fig. 5.

propagate initially as sea-surface reflected phases within the polar half-channel or surface duct, before coupling into the deep sound channel that enables propagation over several thousand kilometres (e.g. at MAD, 5000 km away or at HA08, 6600 km away; e.g. Chapp *et al.* 2005; de Groot-Hedlin *et al.* 2009).

Most cryogenic events (2085) cluster within 100 km from the Antarctic continental shelf (south of the dashed line in Fig. 10). These events may be related to iceberg calving, colliding and rubbing as they drift counter-clockwise around Antarctica within the Antarctic coastal current, which moves counter to the
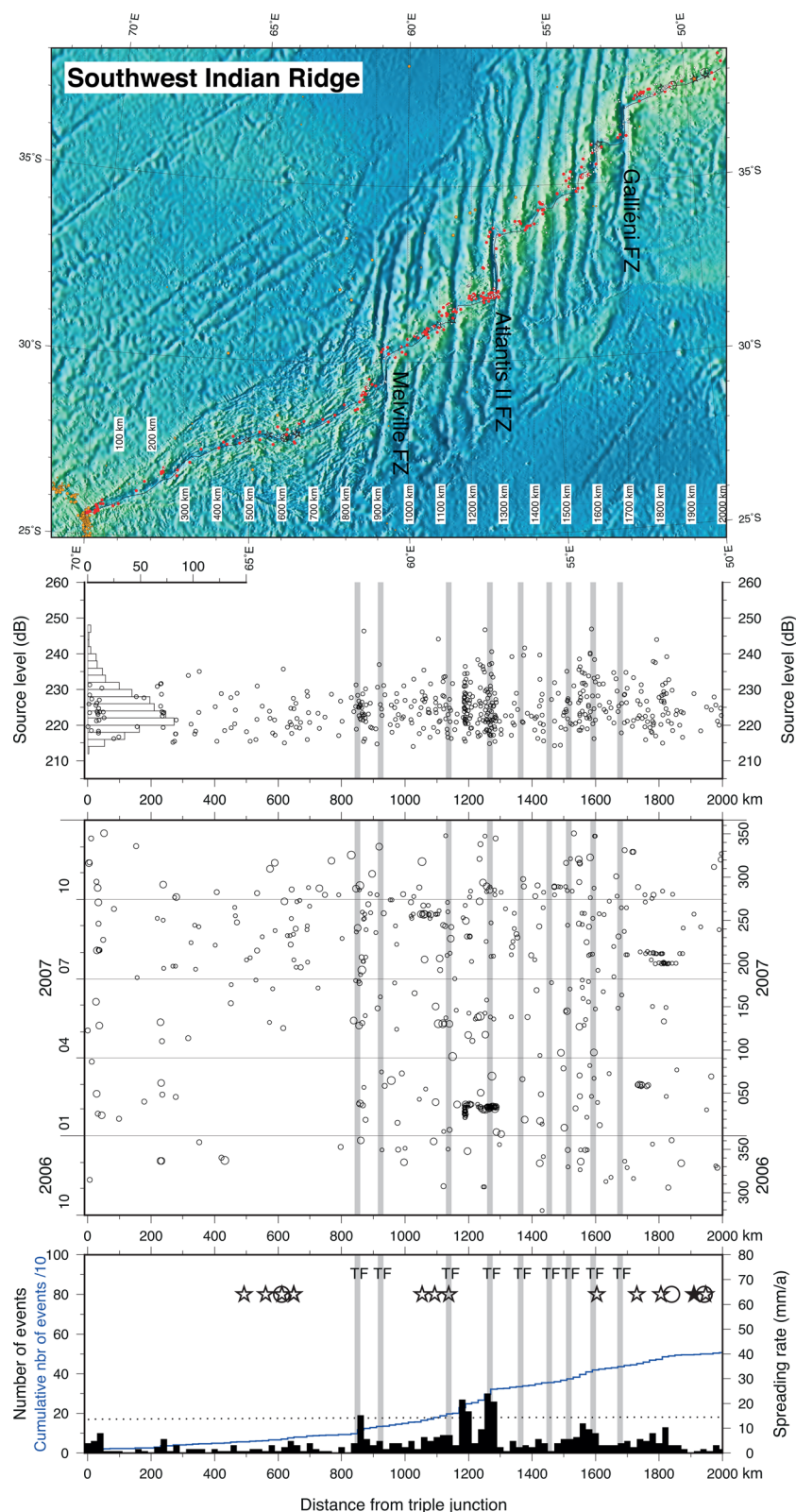
**Figure 6.** Distribution of acoustic events along the (upside-down) Southwest Indian Ridge (SWIR). Same legend as in Fig. 5.

eastward Antarctic Circumpolar Current to the north. Widely distributed events (north of the dashed line) are likely related to drifting icebergs, which sometimes can drift up to 50°S. Each of these events most likely corresponds to one iceberg, which may crack and break into smaller pieces in different locations. The near-shelf clusters reflect a higher density of icebergs and stormy weather periods. The time distribution of the two populations is contrasted (Fig. 11): the near shelf events occur from late Summer to early Spring, in uneven numbers probably depending on the weather (wind and swell), whereas ocean-drifting icebergs mostly
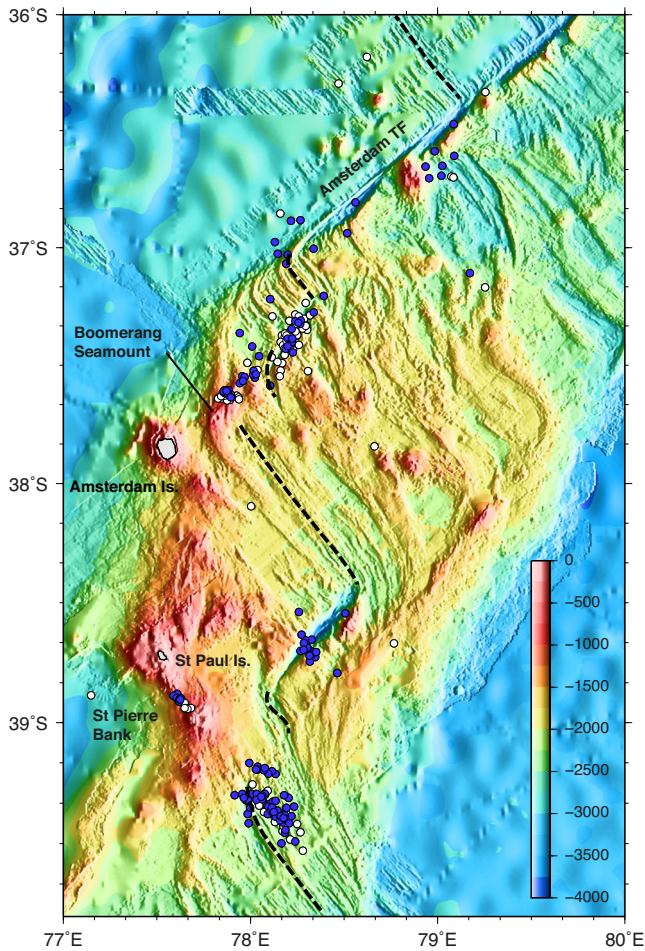
**Figure 7.** Acoustic events (236) over the St Paul and Amsterdam Plateau (Southeast Indian Ridge), detected in 2007 by four or more hydrophones (145 blue symbols) and only three hydrophones (91 white symbols) of the array. Most events cluster on the transform faults that linked the Southeast Indian Ridge segments (dashed lines). One cluster occurs at the tip of the southernmost ridge-axis segment and one cluster is clearly off axis, but associated with a volcanic seamount, the St Pierre bank. Combined bathymetric grids from Scheirer *et al.* (2000) and Maia *et al.* (2011).

crack and disintegrate in the Summer and are much fewer in the Winter.

The source levels of the cryogenic events range from 213 to 245 dB re µPa at 1 m, with a maximum number of events between 220 and 226 dB (Fig. 12). Their distribution is therefore similar to that of the seismic events (Figs 1 and 3), and according to the SL/$m_b$ relationship calculated in a previous section, icequakes produce acoustic source levels equivalent to earthquakes with magnitudes ranging between 2.2 and 3.7 (REB $m_b$). However, it is not possible to assess the completeness of our array or a comparable scale of magnitude. Furthermore, the measured peak-to-peak SL is not always appropriate to characterize cryogenic events. Typically, when the cryogenic signals last several minutes, the operator, in order to locate the event, will pick the arrival times of unique features in the spectrograms (e.g. an impulsive signal onset or interruption, sharp change in frequency). The SL is derived from the maximum peak-to-peak amplitude in a 10s window centred on the picked arrival time. Source levels based on the signal energy in the same 10s window display a similar distribution but shifted towards lower values (205–234 dB range centred on 215). Events located just off
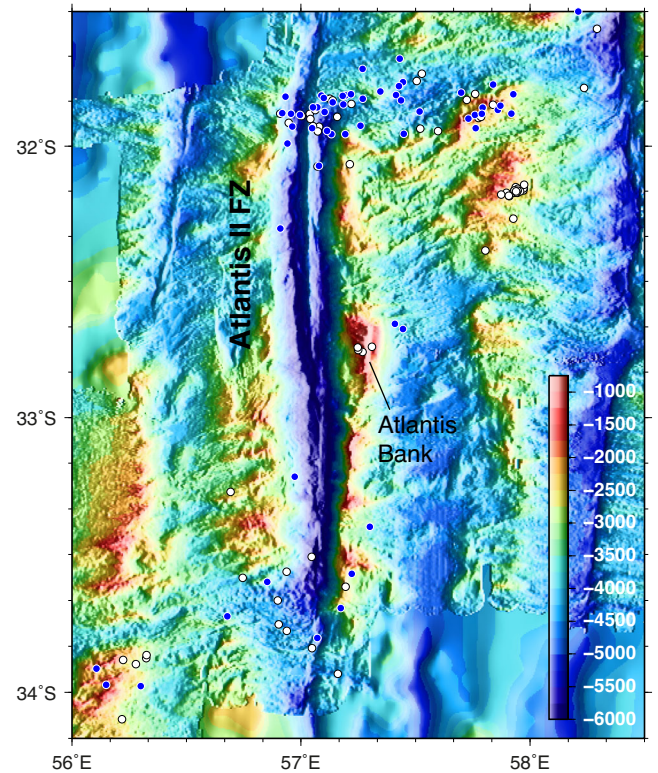


**Figure 8.** Acoustic events near the Atlantis II FZ on the Southwest Indian Ridge, detected in 2007 by four or more hydrophones (57 blue symbols) and only three hydrophones (77 white symbols) of the array. The main cluster of events is located at the northern ridge-transform intersection, but several small clusters occur on off-axis seamounts (see text). Bathymetric grid from Sauter *et al.* (2011).

**Table 3.** Distribution of acoustic events along the Central (CIR), Southeast (SEIR) and Southwest (SWIR) Indian ridges. Length of boundary adds up spreading ridge and transform fault segments.

|  | CIR | SEIR | SWIR |
|---|---|---|---|
| Range of spreading rates (mm a$^{-1}$) | 35–48 | 55–68 | 13–15 |
| Length of boundary (km) | 2119 | 2914 | 2839 |
| Number of events | 809 | 590 | 509 |
| Number of events/100 km | 28 | 20 | 18 |
| Number of events/day | 1.8 | 1.3 | 1.1 |
| Number of events/month | 54 | 39 | 34 |
| Number of events/100 km/month | 1.9 | 1.3 | 1.2 |

the Antarctic margin or from drifting icebergs (i.e. south and north of the dashed line in Fig. 10, resp.) have a similar SL range and distributions. However, events during the austral summer and fall seasons have higher SL than the events during the winter and spring seasons (from 2006 December 1 to 2007 November 31) and they are more frequent (1993 versus 1392 resp.). It suggests that, in this region, the contribution of cryogenic events to the ocean noise budget is higher in the summer and fall than in the winter and spring. This is consistent with seasonal patterns of low-frequency noise observed throughout the Southern Ocean (Matsumoto *et al.* 2014).

## 7 LONG-TERM SOUND SOURCES

Long-term spectrograms of the acoustic power spectral density and the daily average sound levels recorded on the three temporary hydrophones are shown in Fig. 13 (location of the hydrophones is
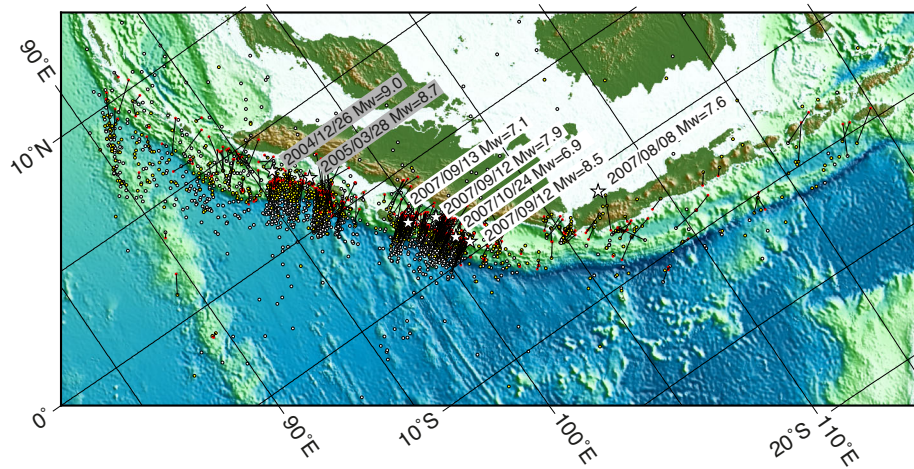
**Figure 9.** Seismicity along the Sunda Trench. Red symbols are epicentres relocated with the Engdahl *et al.* (1998) algorithm (ISC 2011); open white and yellow circles are acoustic events detected by only three and more than three hydrophones, respectively. Bars show the acoustic and seismic matching events. Stars show all events of magnitude $M_w > 6.9$ that occurred in this area during the acoustic experiment; the hypocentres of the Aceh ($M_w = 9.0$; 2004) and Nias ($M_w = 8.7$; 2005) mega-earthquakes have been added for reference.
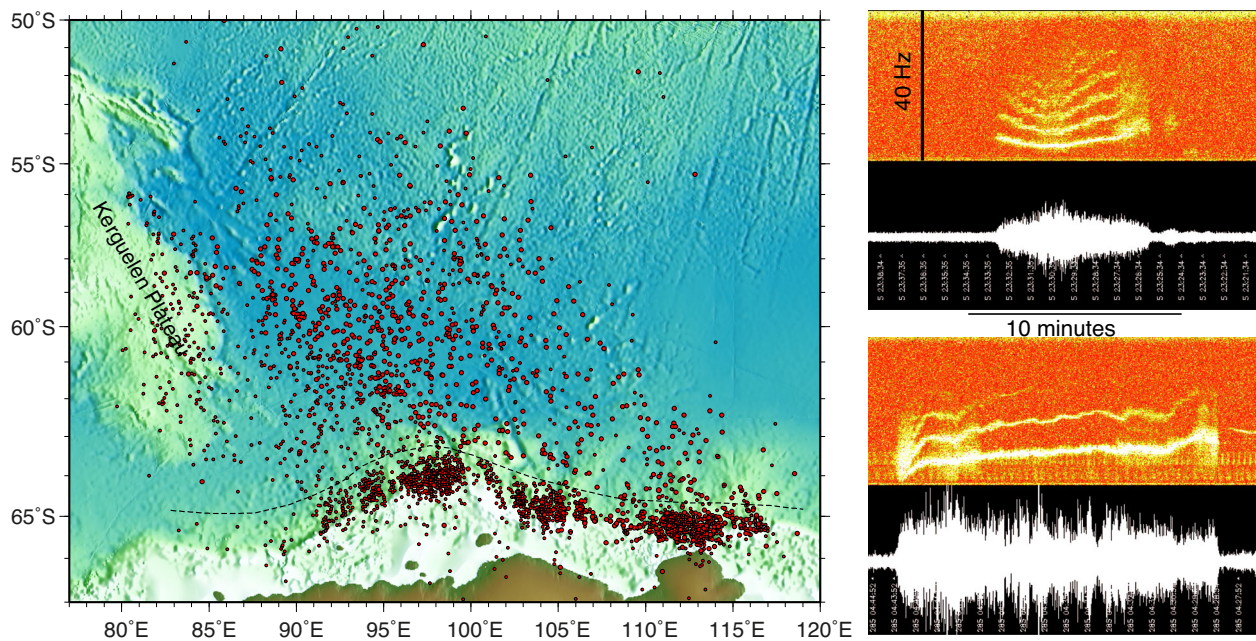


**Figure 10.** Geographic distribution of cryogenic events and examples of ice tremor signatures.

also shown in Fig. 1). Overall, the long-term sound energy levels are roughly equivalent at all three sites, with the background levels in the 70–90 dB re µPa$^2$ Hz$^{-1}$ and the highest energy levels at 110–130 dB re µPa$^2$ Hz$^{-1}$ located in the sub 20 Hz bands. The most sustained source of long-term sounds appears to come from whale vocalizations in the 20–30 and 100 Hz frequency bands, and earthquakes and ice tremor at frequencies <20 Hz.

The acoustic energy on all three hydrophones focused in the 20–30 Hz band with a strong overtone at 100 Hz are the vocalizations of blue (*Balaenoptera musculus*) and fin (*B. physalus*) whales (Širović *et al.* 2004, 2007; Rankin *et al.* 2005; Samaran *et al.* 2013). This energy is present from April to November (2007), which is consistent with the seasonal distribution of these animals, as they appear at lower latitudes during the austral winter. However, the near absence of calls during the austral summer may reflect either

a seasonal migration to other dwelling areas or a seasonal pattern of vocalization. Still the Antarctic blue whales is the most dominant vocalizing whale recorded by the temporary hydrophone array. Other populations of blue whales that contribute to the sound spectra are Sri Lankan, Madagascar and Australian pygmy blue whales (Fig. 13; Samaran *et al.* 2013). Fin whale calls overlap in frequency and time with the blue whales and contribute to the strong baleen whale vocalization energy observed.

At frequencies under 20 Hz, earthquake activity from the Indian Ridges and Java-Sumatra subduction zone, as well as ice-breakup and iceberg grounding sounds sourced near Antarctica, generate broad-band, short-duration impulsive signals that are present throughout the year (Fig. 13) There is also continuous, low-frequency energy present on all three hydrophones under 5 Hz. During several periods of time, which can last from weeks to months,
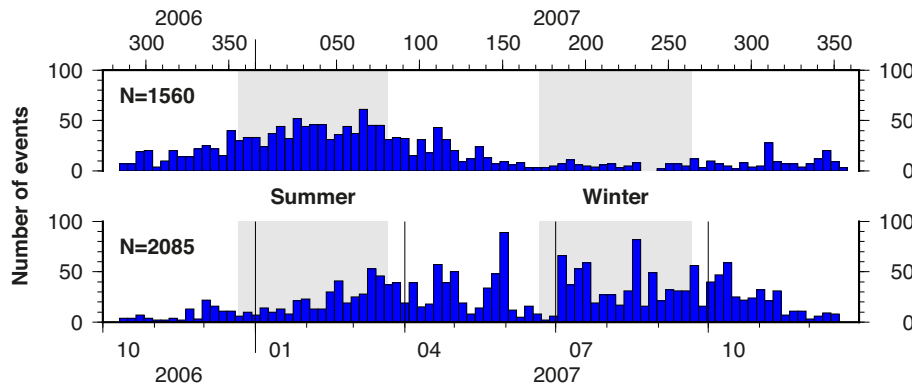
**Figure 11.** Time distribution of cryogenic events over the 2006/2007 season cycle (5 day bin size); *N* is the number of events in each graph; horizontal axes are by months (bottom axis) or Julian days (top axis). Bottom panel: events located within 100 km from the Antarctic continental shelf break (i.e. south of dashed line in Fig. 9). Top panel: events located north of the 100 km limit, mostly related to drifting icebergs.
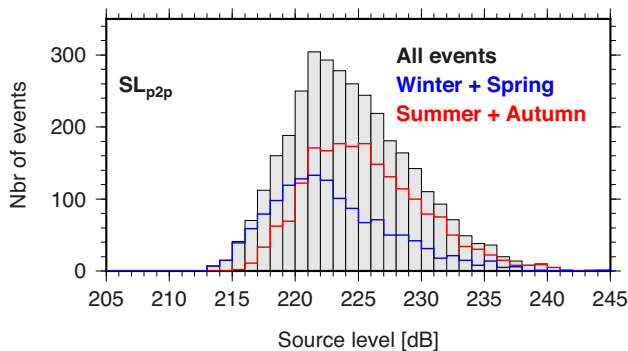


**Figure 12.** Seasonal source-level distribution of cryogenic events from 2006 December 1 to 2007 November 31. The source level is derived from the maximum peak-to-peak amplitude within a 10s window centred on the picked arrival time (see text).

the energy develops into tremor-like signals with a fundamental at 1–3 Hz and several overtones. We interpret this low energy to be from a combination of sources, including broad-band energy created by sea-state (storms, waves and wind), propeller noise from ships in the area, minutes-to-hours long periods of iceberg grounding tremor, as well as periods of tonal 'strumming' caused by fast moving ocean currents that make mooring line vibrate. This low frequency energy remains present throughout the year, which is consistent with the idea that this energy is caused by currents, storms, ships and grounding icebergs that can be present year-round in the Southern Ocean. Moreover, both ships and airgun (for research and/or oil exploration) sounds are frequently present on the Indian Ocean hydrophone data, but we do not see a significant contribution to the long-term noise spectra from these anthropogenic sources as is seen in the north Atlantic and European Arctic (Klinck *et al.* 2012). It is well established that there are much greater levels of ship traffic in the northern hemisphere as compared to the southern hemisphere (Cato 1976).

The southernmost hydrophone exhibits a period of broad-band energy from early June to mid-July 2007. Most of this energy is focused under 20 Hz, although there appears to be a broad overtone from 60 to 80 Hz, thus appearing similar to tremor with a frequency spacing of 40 Hz. It is possible that the signal is an electronic noise introduced by the hydrophone pre-amplifier. However the presence of the tremor-like banding in the signal seems to provide evidence against this explanation. Furthermore, it is not uncommon to observe high frequency (>30 Hz) tremor-like bands

of energy on other hydrophone data recorded throughout the world. These bands have been shown to be a result of interference caused by multipath wide-band signals, including sea-surface and seafloor reflected acoustic phases, that arrive at the hydrophone with small time delays (Matsumoto *et al.* 2011). The multiple arrivals both constructively and destructively interfere based on their arrival polarity, and result in the observed interference pattern. A 40 Hz spacing between energy peaks is due to a 25 ms time delay between a direct path and sea-surface reflected phases. Although we don't know the local bathymetry of the source or, therefore, the exact ray paths, this time delay implies a source depth of a few 10 s to several hundred meters deep assuming a sound velocity of 1490 ms$^{-1}$. This suggests the source of this signal is relatively shallow, which is consistent with a large volcanic source somewhere south of the southernmost SW-AMS hydrophone. Since the signal is only seen on the southern hydrophone, this suggests the source is either (1) close to the southern hydrophone but the signal attenuates before reaching the more distant phones, or (2) the signals are blocked by shallow bathymetry before reaching the distant hydrophones. The best candidate for such a volcanic source would be the St Pierre Bank, 35 km southeast of St Paul Island, which rises to 91 m below sea-level and was the source of 14 events during 2007 March 7 (Fig. 7). Another potential candidate is the Boomerang seamount, an active submarine volcano located north of Amsterdam Island, on the Southeast Indian Ridge axis, with a summit of 650 m depth (Fig. 8; Johnson *et al.* 2000). These active volcanoes are 515 km and 640 km away (respectively) from the SW-AMS hydrophone, while the NE-AMS hydrophone is 965 and 840 km and the MAD hydrophone is 2320 and 2250 km. Thus it is plausible that the more distant hydrophones did not record these volcanic signals because of acoustic attenuation and/or bathymetric shadowing.

## 8 CONCLUSION

The Deflo-hydroacoustic experiment, supplemented by the IMS permanent hydroacoustic stations in Diego Garcia Island and Cape Leeuwin, provides a 14-month continuous window on the Indian Ocean soundscape, from whale vocalizations in the 20–30 and 100 Hz frequency bands, to earthquakes and ice tremors at frequencies <20 Hz. Man-made sounds such as ships or seismic surveys are also present, but only a minor contribution to the overall ambient sound levels. Due to the hydrophone sensitivity and to the acoustic properties of the ocean, the completeness of the acoustic/seismic catalogue is on the order of $m_b$ 3.2 with a threshold of $m_b$ 2.6, leading to the
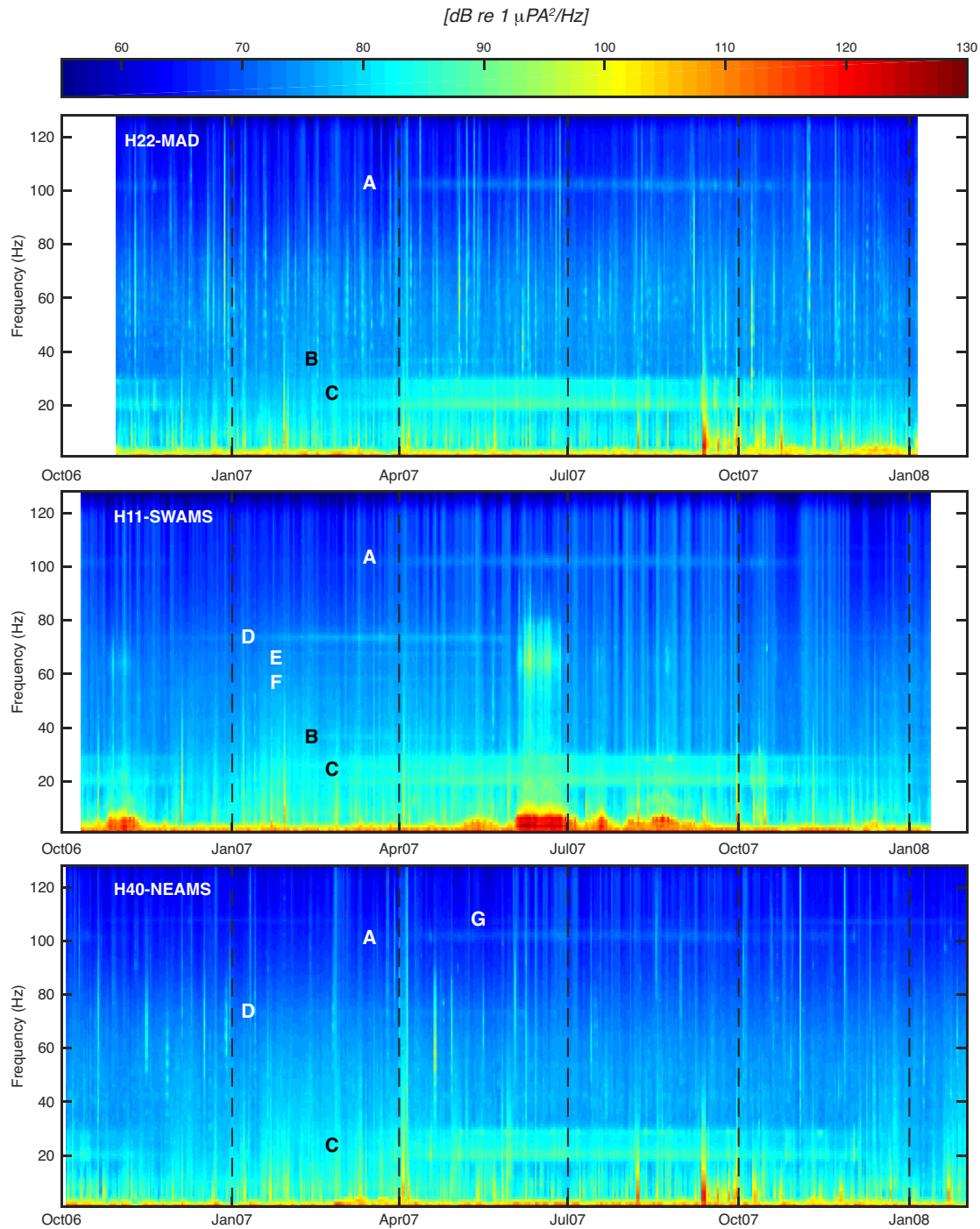
**Figure 13.** Annual spectrograms of the three temporary hydrophones (location on Fig. 1). Each vertical line is a 24 hr average spectrogram. High-energy bursts, between 0 and 20 Hz, are due to earthquakes, volcanic tremors and cryogenic events. Horizontal lines correspond to whale vocalizations at very specific frequencies: (a) fin whales at ∼100 Hz, (b) Madagascan pygmy blue whales at ∼37 Hz, (c) Antarctic blue whales at 18–28 Hz, (d) Australian pygmy blue whales near 72 Hz, (e) 67 Hz, (f) and 57 Hz, (g) pygmy blue whales from Sri Lanka at 106 Hz. The horizontal extent of the lines shows their seasonal presence at the three locations. The five species and subspecies all travel to the southern-most site (H11). Fin whales and Antarctic blue whales are ubiquitous and mostly present from April to October. Madagascan pygmy blue whales are observed at the western sites (H20, H11), Australian and Sri Lanka blues are observed at the eastern sites (H11, H40).

detection of 5–16 times more events than reported by land-based networks. The main sources of seismic events are the Sunda Trench and the three Indian spreading ridges, which are well covered by the hydrophone array. The low-level seismicity associated with the ridges shows contrasted distribution depending on the spreading rate. The Southeast Indian Ridge, the fastest spreading of the three ridges (55–68 mm $a^{-1}$), displays seismic activity mainly focused on transform faults and near the St Paul and Amsterdam hotspots. The slow-spreading Central (35–48 mm $a^{-1}$) and ultraslow spreading Southwest (13–15 mm $a^{-1}$) Indian ridges display more evenly

distributed events between ridge segment and transform faults. Cryogenic events are a significant component of the Indian Ocean noise budget, with high source levels and a latitude-dependent seasonal contribution. Whale vocalizations from five different species and subspecies (fin whale, Antarctic blue whale and pygmy blue whales from Madagascar, Australia and Sri Lanka) are also present near each hydrophone of the array, and their acoustic energy levels show clear seasonal variability. Monitoring over several seasonal cycles may provide insight on the population distributions and migration patterns of these whale species. It is apparent that long-term acoustic monitoring of the ocean, particularly in the remote Southern Ocean, may offer a wealth of new information on a variety of marine geophysical and ecosystem issues and can be accomplished using only a few widely spaced instruments.

## REFERENCES

Baines, A.G., Cheadle, M.J., Dick, H.J.B., Scheirer, A.H., John, B.E., Kusznir, N.J. & Matsumoto, T., 2003. Mechanism for generating the anomalous uplift of oceanic core complexes: Atlantis Bank, southwest Indian Ridge, *Geology,* **31,** 1105–1108.

Beaulieu, S.E., 2013. Version 3.2: InterRidge global database of active submarine hydrothermal vent fields, Available at: http://vents-data.interridge.org, last accessed 1 August 2013.

Bergman, E.A., Nabelek, J.L. & Solomon, S.C., 1984. An extensive region of off-ridge normal-faulting earthquakes in the southern Indian Ocean, *J. geophys. Res.,* **89,** 2425–2443.

Bohnenstiehl, D.R. & Tolstoy, M., 2003. Comparison of teleseismically and hydroacoustically derived earthquake locations along the North-central Mid-Atlantic Ridge and Equatorial East Pacific Rise, *Seism. Res. Lett.,* **74,** 791–802.

Bohnenstiehl, D.R., Tolstoy, M., Dziak, R.P., Fox, C.G. & Smith, D.K., 2002. Aftershock sequences in the mid-ocean ridge environment: an analysis using hydroacoustic data, *Tectonophysics,* **354,** 49–70.

Bohnenstiehl, D.R., Tolstoy, M., Smith, D.K., Fox, C.G. & Dziak, R.P., 2003. Time-clustering behavior of spreading-center seismicity between 15 and 35 degrees N on the Mid-Atlantic Ridge: observations from hydroacoustic monitoring, *Phys. Earth planet. Int.,* **138,** 147–161.

Cato, D.H., 1976. Ambient sea noise in waters near Australia, *J. acoust. Soc. Am.,* **60,** 320–328.

Chapp, E., Bohnenstiehl, D.R. & Tolstoy, M., 2005. Sound-channel observations of ice-generated tremor in the Indian Ocean, *Geochem. Geophys. Geosyst.,* **6,** Q06003, doi:10.1029/2004GC000889.

Conder, J.A., Scheirer, D.S. & Forsyth, D.W., 2000. Seafloor spreading on the Amsterdam-St Paul hotspot plateau, *J. geophys. Res.,* **105,** 8263–8277.

Cowie, P.A., Scholz, C.H., Edwards, M. & Malinverno, A., 1993. Fault strain and seismic coupling on mid-ocean ridges, *J. geophys. Res.,* **98,** 17 911–17 920.

de Groot-Hedlin, C., Blackman, D.K. & Jenkins, C.S., 2009. Effects of variability associated with the Antarctic circumpolar current on sound propagation in the ocean, *Geophys. J. Int.,* **176,** 478–490.

DeMets, C., Gordon, R.G., Argus, D.F. & Stein, S., 1994. Effect of recent revisions to the geomagnetic reversal timescale on estimates of current plate motion, *Geophys. Res. Lett.,* **21,** 2191–2194.

Dziak, R.P. *et al.*, 2004. P- and T-wave detection thresholds, Pn velocity estimate, and detection of lower mantle and core P-waves on ocean sound-channel hydrophones at the Mid-Atlantic Ridge, *Bull. seism. Soc. Am.,* **94,** 665–677.

Dziak, R.P., Hammond, S.R. & Fox, C.G., 2011. A 20-year hydroacoustic time series of seismic and volcanic events in the northeast Pacific Ocean, *Oceanography,* **24,** 280–293.

Dziak, R.P., Bohnenstiehl, D.R. & Smith, D.K., 2012. Hydroacoustic monitoring of oceanic spreading centers: past, present, and future, *Oceanography,* **25,** 116–127.

Engdahl, E.R., van der Hilst, R.D. & Buland, R.P., 1998. Global teleseismic earthquake relocation with improved travel times and procedures for depth determination, *Bull. seism. Soc. Am.,* **88,** 722–743.

Escartin, J., Smith, D.K., Cann, J., Schouten, H., Langmuir, C.H. & Escrig, S., 2008. Central role of detachment faults in accretion of slow-spreading oceanic lithosphere, *Nature,* **455,** 790–795.

Fox, C.G. & Dziak, R.P., 1998. Hydroacoustic detection of volcanic activity on the Gorda Ridge, February-March 1996, *Deep Sea Res.,* **45,** 2513–2530.

Fox, C.G., Radford, W.E., Dziak, R.P., Lau, T.K., Matsumoto, H. & Schreiner, A.E., 1995. Acoustic detection of a seafloor spreading episode on the Juan-de-Fuca Ridge using military hydrophone arrays, *Geophys. Res. Lett.,* **22,** 131–134.

Fox, C.G., Matsumoto, H. & Lau, T.-K.A., 2001. Monitoring Pacific Ocean seismicity from an autonomous hydrophone array, *J. geophys. Res.,* **106,** 4183–4206.

Gavrilov, A. & Li, B., 2008. Long term variations of ice breaking noise in Antarctica, in *Proceedings of the Acoustics'08,* Abstract 1PAOA3, Paris.

Goslin, J., Lourenco, N., Dziak, R.P., Bohnenstiehl, D.R., Haxel, J. & Luis, J., 2005. Long-term seismicity of the Reykjanes Ridge (North Atlantic) recorded by a regional hydrophone array, *Geophys. J. Int.,* **162,** 516–524.

Goslin, J. *et al.*, 2012. Spatiotemporal distribution of the seismicity along the Mid-Atlantic Ridge north of the Azores from hydroacoustic data: insights into seismogenic processes in a ridge-hot spot context, *Geochem. Geophys. Geosyst.,* **13,** Q02010, doi:10.1029/2011GC003828.

Gutenberg, B. & Richter, C.F., 1954. *Seismicity of the Earth and Associated Phenomena,* Princeton Univ. Press, Princeton, NJ.

Hanson, J.A. & Bowman, J.R., 2005. Indian Ocean ridge seismicity observed with a permanent hydroacoustic network, *Geophys. Res. Lett.,* **32,** 1–4.

Hanson, J.A. & Bowman, J.R., 2006. Methods for monitoring hydroacoustic events using direct and reflected T waves in the Indian Ocean, *J. geophys. Res.,* **111,** B02305, doi:10.1029/2004JB003609.

Hashimoto, J., Ohta, S., Gamo, T., Chiba, H., Yamaguchi, T., Tsuchida, S., Okudaira, T., Watabe, H., Yamanaka, T. & Kitazawa, M., 2001. First hydrothermal vent communities from the Indian Ocean discovered, *Zool. Sci.,* **18,** 717–721.

Hildebrand, J.A., McDonald, M.A. & Webb, S.C., 1997. Microearthquakes at intermediate spreading-rate ridges: the Cleft segment megaplume site on the Juan de Fuca Ridge, *Bull. seism. Soc. Am.,* **87,** 684–691.

International Seismological Centre (ISC), 2011. On-line bulletin, Available at: http://www.isc.ac.uk, last accessed 25 June 2013.

Johnson, K.T.M., Graham, D.W., Rubin, K.H., Nicolaysen, K., Scheirer, D.S., Forsythe, D.W., Baker, E.T. & Douglas-Priebe, L.M., 2000. Boomerang Seamount: the active expression of the Amsterdam-St. Paul hotspot, Southeast Indian Ridge, *Earth planet. Sci. Lett.,* **183,** 245–259.

Klinck, H., Nieukirk, S.L., Mellinger, D.K., Klinck, K., Matsumoto, H. & Dziak, R.P., 2012. Seasonal presence of cetaceans and ambient noise levels in polar waters of the North Atlantic, *J. acoust. Soc. Am. - Express Letters,* **132**(3), doi:10.1121/1.4740226.

Lay, T. *et al.*, 2005. The great Sumatra-Andaman earthquake of 26 December 2004, *Science,* **308,** 1127–1133.

Macdonald, K.C. & Mudie, J.D., 1974. Microearthquakes on Galapagos spreading center and seismicity of fast-spreading ridges, *Geophys. J. R. astr. Soc.,* **36,** 245–257.

Maia, M. *et al.*, 2011. Building of the Amsterdam-Saint Paul plateau: a 10 Myr history of a ridge-hot spot interaction and variations in the strength of the hot spot source, *J. geophys. Res.: Solid Earth,* **116,** B09104, doi:10.1029/2010JB007768.

Matsumoto, H., Bohnenstiehl, D.R., Dziak, R.P., Park, M. & Embley, R.W., 2011. Use of an Autonomous Hydrophone Array to Assess Hydroacoustic Propagation through the ACZ and Blockage by the Islands and Bathymetric Ridges in the Scotia Sea, in Final Technical Report, Nuclear Explosion Monitoring Research and Engineering (NEMR&E) Program.

Matsumoto, H., Bohnenstiehl, D.R., Tournadre, J., Dziak, R.P., Haxel, J.H., Lau, T.-K.A., Fowler, M. & Salo, S.A., 2014. Antarctic icebergs: a significant natural ocean sound source in the Southern Hemisphere, *Geochem. Geophys. Geosyst.,* **15**(8), 3448–3458.

Michon, L., Staudacher, T., Ferrazzini, V., Bachelery, P. & Marti, J., 2007. April 2007 collapse of Piton de la Fournaise: a new example of caldera formation, *Geophys. Res. Lett.,* **34,** doi:10.1029/2007GL031248.

Pan, J.F. & Dziewonski, A.M., 2005. Comparison of mid-oceanic earthquake epicentral differences of travel time, centroid locations, and those determined by autonomous underwater hydrophone arrays, *J. geophys. Res.,* **110,** B07302, doi:10.1029/2003JB002785.

Petroy, D.E. & Wiens, D.A., 1989. Historical seismicity and implications for diffuse plate convergence in the northeast Indian Ocean, *J. geophys. Res.,* **94,** 12 301–12 319.

Rankin, S., Ljungblad, D., Clark, C. & Kato, H., 2005. Vocalisations of Antarctic blue whales, Balaenoptera musculus intermedia, recorded during the 2001/2002 and 2002/2003 IWC/SOWER circumpolar cruises, Area V, Antarctica, *J. Cetacean Res. Manag.,* **7,** 13–20.

Royer, J.-Y. & Gordon, R.G., 1997. The motion and boundary between the Capricorn and Australian plates, *Science,* **277,** 1268–1274.

Royer, J.-Y. & Schlich, R., 1988. The Southeast Indian Ridge between the Rodriguez Triple Junction and the Amsterdam and Saint-Paul Islands: detailed kinematics for the past 20 Ma, *J. geophys. Res.,* **93,** 13 524–13 550.

Samaran, F., Stafford, K.M., Branch, T.A., Gedamke, J., Royer, J.Y., Dziak, R.P. & Guinet, C., 2013. Seasonal and geographic variation of southern blue whale subspecies in the Indian Ocean, *Plos One,* **8,** 10.

Sauter, D., Sloan, H., Cannat, M., Goff, J., Patriat, P., Schaming, M. & Roest, W.R., 2011. From slow to ultra-slow: how does spreading rate affect seafloor roughness and crustal thickness?, *Geology,* **39,** 911–914.

Sauter, D. *et al.*, 2013. Continuous exhumation of mantle-derived rocks at the Southwest Indian Ridge for 11 million years, *Nat. Geosci.,* **6,** 314–320.

Scheirer, D.S., Forsyth, D.W., Conder, J.A., Eberle, M.A. & Hung, S.-H., 2000. Anomalous seafloor spreading of the Southeast Indian Ridge near the Amsterdam-St Paul Plateau, *J. geophys. Res.,* **105,** 8243–8262.

Schlich, R., 1982. The Indian Ocean: aseismic ridges, spreading centers and basins, in *The Indian Ocean,* pp. 51–147, eds Nairn, A.E.M. & Stehli, F.G., Plenum Press.

Simão, N., Escartin, J., Goslin, J., Haxel, J., Cannat, M. & Dziak, R., 2010. Regional seismicity of the Mid-Atlantic Ridge: observations from autonomous hydrophone arrays, *Geophys. J. Int.,* **183,** 1559–1578.

Širović, A., Hildebrand, J.A., Wiggins, S.M., McDonald, M.A., Moore, S.E. & Thiele, D., 2004. Seasonality of blue and fin whale calls and the influence of sea ice in the Western Antarctic Peninsula, *Deep-Sea Res. II,* **51,** 2327–2344.

Širović, A., Wiggins, S.M. & Hildebrand, J.A., 2007. Blue and fin whale call source levels and propagation range in the Southern Ocean, *J. acoust. Soc. Am.,* **122,** 1208–1215.

Smith, D.K., Tolstoy, M., Fox, C.G., Bohnenstiehl, D.R., Matsumoto, H. & Fowler, M., 2002. Hydroacoustic monitoring of seismicity at the slow-spreading Mid-Atlantic Ridge, *Geophys. Res. Lett.,* **29**(11), doi: 10.1029/2001GL013912.

Storchak, D.A., Bondar, I., Harris, J. & Dando, B., 2011. CTBTO contribution to the global earthquake data collection: a view from the International Seismological Centre (ISC), in *Proceedings of the CTBTO Science and Technology Conference,* Vienna, Austria.

Stroup, D.F., Bohnenstiehl, D.R., Tolstoy, M., Waldhauser, F. & Weekly, R.T., 2007. Pulse of the seafloor: tidal triggering of microearthquakes at 9°50′N East Pacific Rise, *Geophys. Res. Lett.,* **34,** L15301, doi:10.1029/2007GL030088.

Talandier, J., Hyvernaud, O., Okal, E.A. & Piserchia, P.F., 2002. Long-range detection of hydroacoustic signals from large icebergs in the Ross Sea, Antarctica, *Earth planet. Sci. Lett.,* **203,** 519–534.

Talandier, J., Hyvernaud, O., Reymond, D. & Okal, E.A., 2006. Hydroacoustic signals generated by parked and drifting icebergs in the Southern Indian and Pacific Oceans, *Geophys. J. Int.,* **165,** 817–834.

Tamaki, K., 2010. Dodo field and solitaire field: newly discovered hydrothermal fields at the Central Indian Ridge, in *Proceedings of the AGU Fall Meeting,* Abstract OS21A-1468, American Geophysical Union, San Francisco, CA.

Tolstoy, M. & Bohnenstiehl, D., 2006. Hydroacoustic contributions to understanding the December 26th 2004 great Sumatra-Andaman Earthquake, *Surv. Geophys.,* **27**(6), 633–646.

Van Dover, C.L. *et al.*, 2001. Biogeography and ecological setting of Indian Ocean hydrothermal vents, *Science,* **294,** 818–823.

Wessel, P. & Smith, W.H.F., 1998. New, improved version of Generic Mapping Tools released, *EOS, Trans. Am. geophys. Un.,* **79,** 579.

Wiens, D.A., 1986. Historical seismicity near Chagos: a complex deformation zone in the equatorial Indian Ocean, *Earth planet. Sci. Lett.,* **76,** 350–360.